Advanced Materials Science and Technology Vol 5 Issue 1 2023
DOI: 10.37155/2717–526X–0501–3

ORIGINAL RESEARCH ARTICLE

Open Access

Omniscient Pte.Ltd.

Optical Properties of the Crystalline Silicon-black Silicon-perovskite Tandem Solar Cells

Ferdinand Gasparyan[1,2,*]

[1]Yerevan State University, 1, Alex Manoogian St., Yerevan 0025, Armenia.
[2]National Polytechnic University of Armenia, 105, Teryan St, Yerevan 0009, Armenia.

***Correspondence to:** Ferdinand Gasparyan, Yerevan State University, 1, Alex Manoogian St., Yerevan 0025, Armenia. Email: fgaspar@ysu.am

Received: June 19, 2023; **Accepted:** August 15, 2023; **Published Online:** August 25, 2023

Citation: Gasparyan F. Optical Properties of the Crystalline Silicon-black Silicon-perovskite Tandem Solar Cells. *Advanced Materials Science and Technology*, 2023;5(1):0517626. https://doi.org/10.37155/2717-526X-0501-3

Abstract: The optical properties of a tandem three-layered structure of crystalline silicon-black silicon-perovskite have been theoretically studied for using it in solar energy conversion. The transfer matrix method is used for obtaining the analytical expressions for the reflection, transmission, and absorption coefficients. It is shown that the transfer matrix method can be successfully applied to the more complicated case of three layers with complex refractive indexes. Numerical calculations performed at an angle of incidence of radiation of 60° showed that in the region of short wavelengths the reflection coefficient takes on low values (several percent), which gradually increase and become > 10% at wavelengths above 0.8 μm. The theoretically modeled results of the reflection coefficient are in good agreement with experimental data carried out for the structures crystalline silicon-black silicon-TiO_2-perovskite. The discrepancy between the experimental and model data slowly increases with increasing wavelength. The transmittance was extremely low and increased slowly with the increasing wavelength. It is found that cheaper and easier created tandem crystalline silicon-black silicon-perovskite structure may have the potential for solar energy conversion.

Keywords: Perovskite; Black silicon; Transfer matrix method; Optical properties; Solar cell

1. Introduction

The efficiency of silicon solar cells (SC) is partly limited by its high refractive index[1]. Silicon, an indirect band gap semiconductor, has a reflectance of approximately 30% in the visible wavelength range. To improve the performance of silicon SCs, it is necessary to minimize reflection loss and increase absorption. The Fresnel reflection loss that occurs at the interfaces between materials with different refractive indices depends on the difference in the refractive indices of the layers. The use of antireflection coatings (ARC) with a gradient profile of the refractive index contributes to an increase in absorption of the SC[2]. Note also that decrease in the reflection of light

at the interfaces will significantly affect the efficiency and consequently, the cost of the solar panels.

Black silicon (b-Si), when used instead of or in conjunction with crystalline silicon (c-Si), makes it possible to increase the absorption of light at visible and near-infrared wavelengths. Black Si has very low reflectivity in the visible range of wavelengths[3-6]. Owing to its morphology, b-Si effectively suppresses reflection and simultaneously enhances light scattering and absorption. The improved light absorption and reduced reflectivity of b-Si make it promising candidate for SC. As the effective refractive index of the b-Si layers (1.1-1.3) is lower than that of c-Si (3.8), it can also be used as an ARC for c-Si SCs[4]. A synthetic method for studying the optical properties of b-Si was presented in Ref. [3]. The technology of manufacturing nanostructures, modeling method for explaining the structural features of the sample, study of the relationship between nanostructures and optical properties of b-Si, and distribution of light intensity in surface textures are presented in detail. The study of the optical properties of b-Si by modeling and their comparison with the model and experimental optical properties of b-Si and c-Si was carried out in Ref. [7]. The transmittance of b-Si is very low for all thicknesses compared to that of c-Si. Gradual development of the real and imaginary parts of the complex index of refraction was observed in b-Si layers[8]. The reflectance of the sample was strongly influenced by an increase in the thickness of the b-Si layer. For 10 μm thickness b-Si layer, the reflectance was below 1% and was very close to zero. For the c-Si/b-Si tandem, the influence of changes in the b-Si thickness on the reflectance of the multilayer was absent, and in the wavelength range of 0.4-1.0 μm, the reflectance changed almost uniformly[8].

Recently, the creation and intensive comprehensive study of organic, inorganic, and mixed perovskite (PVK) materials have contributed to their use in SCs. Perovskite SCs have significant potential as the top cell in a tandem structure with c-Si as the bottom cell. The band-gap and refractive index of PVK are optimal for using in SCs. In Refs. [9-14], various PVK materials and the dependence of the band-gap energy on the refractive index were studied. A simple empirical relationship between the band-gap energy and refractive index for PVK was developed and proposed. Due to the wider band gap of PVK (1.56-1.65 eV) than that of b-Si (1.54 eV[15]) and c-Si (1.12 eV), its absorption spectrum is shifted to a short-wavelength region of the spectrum, where the absorption of b-Si and c-Si is lower.

One of the methods to broaden the spectral response range and upgrade the performance of an established PVK SC is to combine the narrow band gap c-Si absorber under the PVK SC to make a tandem SC[16-18]. Top cells comprising a wide band gap semiconductor generate photocurrent at high voltage from the short-wavelength part of the solar spectrum. Longer wavelength light, beyond the band gap of the top cell, is transmitted to an underlying bottom cell comprising a narrow band gap semiconductor with a broad absorption coefficient. To maximize light coupling into the bottom SC, the Si surface is typically textured in random pyramids or grooves by mask-less wet etching technology[19-23]. Whereas the flat substrates have enormous reflection losses, the textured surfaces enable improved light coupling into the Si SCs. The highest efficiency values of 33.7% were observed for PVK-Si SCs[24] and > 29% for PVK-Si tandem SCs with a textured surface[19]. For the perovskite/silicon tandem featuring a b-Si with a tunnel oxide passivated contact subcell a 28.2% efficiency were observed[25]. Studies show that for achieving the lowest reflection value of Si substrates, the most effective solution is the use of nanotextured surfaces, in particular, from b-Si[26-28]. A preliminary estimate of the optical properties of the tandem c-Si/b-Si/PVK in the absence of optical losses is given in our previous work[29]. However, for real structures, it is important to model these properties taking into account the complex refractive index (real and imaginary parts) of constituent layers. Some results of the experimental study and modeling of the optical properties of the c-Si/b-Si/PVK structure, carried out by us, have been published recently in Ref. [30].

Currently, some major modeling methods are commonly used in the field of AR sub-wavelength structures, such as the finite-difference time-domain (FDTD), finite element method (FEM), transfer matrix method (TMM), and rigorous coupled-wave analysis or Fourier modal method (RCWA/FMM)[31]. TMM is also used to study the wave transmission in one-dimensional structures and allows one to calculate band diagrams, reflection and transmission spectra, emission spectra[31], guided modes, and the modeling of porosity and thickness gradients[32]. For example, TMM was used to

simulate a seven-layer ARC[33]. When measuring the reflectivity of thin film ARCs, the TMM is a fast and simple simulation method. It is capable of calculating reflectance and transmittance, and can handle multiple wavelengths, dispersion, and multiple angles of incidence irradiation. TMM also handle absorption through layers with complex refractive indices. The TMM has also been used for modeling and numerical optical optimization of planar tandem c-Si/PVK SCs with regular and inverted device architectures[34-36]. There are currently several commercially available programs using the TMM, including FreeSnell, EMPy, Luxpop.com and Thinfilm, *etc*.

The aim of this work is theoretically modeling the optical properties (reflection, transmission, and absorption) of a c-Si/b-Si/PVK tandem structure using TMM, demonstrating the acceptability of this method for a three-layer structure with complex refractive indices of the layers and to revealing the possibility of efficient use of such structure for the conversion of solar energy.

2. Theory and Simulation

The energy diagram of the tandem c-Si/b-Si/PVK structure under study at equilibrium is shown in Figure 1. Here, E_C and E_V are the lower energy of the conduction band and the upper energy of the valence band, respectively, E_F is the Fermi level energy, ETM and HTM are the electron and hole transfer materials, respectively, and RJ is the recombination junction. The black and empty cycles show the holes and electrons, respectively. In the followings, for the numerical calculations, we use the parameters of halide PVK ($CH_3NH_3PbI_3$), TiO_2 as ETM and NiO as HTM. To construct the energy diagram, we used the following knowledge for the energy of the band gap (E_g), the affinity (χ) and discontinuities in the conduction and valence bands (ΔE_C, ΔE_V) of materials:

$\chi_{cSi} = 4.05\,\text{eV}$[37]; $\chi_{bSi} = 3.65\,\text{eV}$[38] [1]; $\chi_{PVK} = 3.9\,\text{eV}$[39]; ($\chi_{PVK} = 3.73\,\text{eV}$[21]);
$\chi_{TiO_2} = 4.1\,\text{eV}$[40]; $\chi_{NiO} = 1.8\,\text{eV}$[41];
$E_{g,cSi} = 1.12\,\text{eV}$[37]; $E_{g,bSi} = 1.52\,\text{eV}$[15]; $E_{g,PVK} = 1.62\,\text{eV}$[39];
$E_{g,TiO_2} = 3.1\,\text{eV}$[42]; $E_{g,NiO} = 3.86\,\text{eV}$[40];
$\Delta E_{C1} = \chi_{bSi} - \chi_{cSi} = 3.65 - 4.05 = -0.4\,\text{eV}$;
$\Delta E_{V1} = E_{g,bSi} - E_{g,cSi} - \Delta E_{C1} = 1.52 - 1.12 - (-0.4) = 0.8\,\text{eV}$;
$\Delta E_{C2} = \chi_{TiO_2} - \chi_{bSi} = 4.1 - 3.65 = 0.45\,\text{eV}$;
$\Delta E_{V2} = E_{g,TiO_2} - E_{g,bSi} - \Delta E_{C2} = 3.1 - 1.52 - 0.45 = 1.13\,\text{eV}$;
$\Delta E_{C3} = \chi_{PVK} - \chi_{TiO_2} = 3.9 - 4.1 = -0.2\,\text{eV}$;
$\Delta E_{V3} = E_{g,PVK} - E_{g,TiO_2} - \Delta E_{C3} = 1.62 - 3.1 - (-0.2) = -1.28\,\text{eV}$;
$\Delta E_{C4} = \chi_{NiO} - \chi_{PVK} = 1.8 - 3.9 = -2.1\,\text{eV}$;
$\Delta E_{V4} = E_{g,NiO} - E_{g,PVK} - \Delta E_{C4} = 3.86 - 1.62 - (-2.1) = 4.34\,\text{eV}$

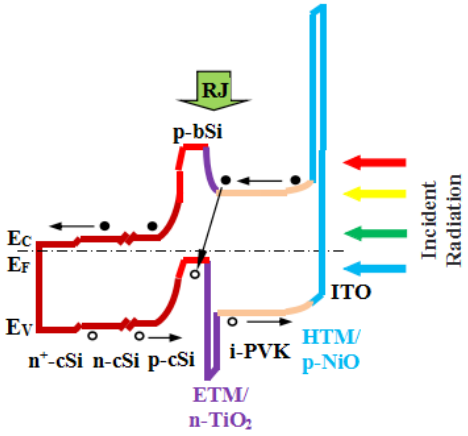

Figure 1. The investigated tandem c-Si/ b-Si/ PVK structure at the equilibrium

[1] Assuming that some parameters (for example, work function, and electron affinity) for b-Si and porous Si are approximately the same, we can take $\chi_{bSi} = 3.65\,\text{eV}$[38].

Under the action of the incident radiation, multiple reflections occur inside the structure. For further theoretical modeling of such a three-layer structure, we represent each layer with its complex refractive index and corresponding thickness **(Figure 2**). On **Figure 2** shows the investigated three-layer structure c-Si/b-Si/PVK (a) and its schematic representation (b), where d = 100 nm, l = 150 nm[5]. Other data noted in **Figure 2a** are presented in paragraph 3. As noted in Ref. [29], such a geometric transformation of a real structure can effectively reflect the features of the reflection, transmission and acceptance of external radiation. The optical properties of such three-layer structure can be easily investigated using the TMM. If electromagnetic radiation is directed onto a structure formed by layers of different materials, multiple reflections occur within the structure. The idea is to describe each layer with a 2×2 matrix, which comes from the boundary conditions for the electromagnetic fields. The most general principle for calculating the reflectance and transmittance of multilayer structure by TMM is based on the matrix formulation of the boundary conditions of the layer interfaces derived from Maxwell's equations[43,44]. Notably, this method accounts for the cumulative effects of light reflected at each interface. Within the framework of this method, it is impossible to take into account the peculiarities of the regular nipple arrays on the surface of b-Si.

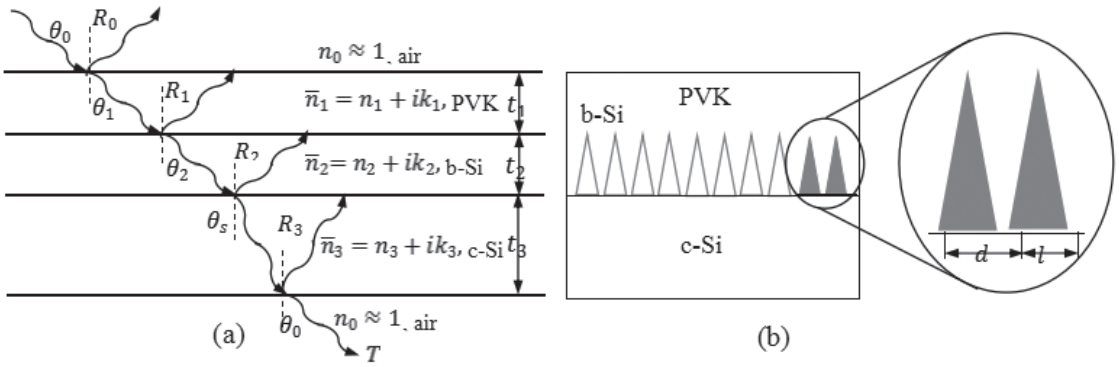

Figure 2. The investigated three-layer structure c-Si/b-Si/PVK (a) and its schematic representation (b)

It can be shown that the optical properties of the three-layered structure can be represented by a 2×2 matrix[45]:

$$M_j = \begin{pmatrix} cos\delta_j & isin\delta_j/\gamma_j \\ i\gamma_j sin\delta_j & cos\delta_j \end{pmatrix} \quad (1)$$

where the phase angle

$$\delta_j = \frac{2\pi}{\lambda}\delta_j = \frac{2\pi}{\lambda}\left(\overline{n_j}t_j\cos\theta_j\right), \gamma_j = \overline{n_j}\cos\theta_j, \overline{n_j} = n_j + ik_j, j = 0,1,2,3 \quad (2)$$

The quantity $\overline{n_j}t_j cos\theta_j$ is called the "effective optical thickness" of the layer for an angle of refraction θ_j; t_j is the thickness of the corresponding j-th layer, and the γ_j effective refractive index, which, for incident radiation perpendicular to the surface of the structure under study, n_j and k_j are the real and imaginary parts of the complex refractive index for the corresponding j-th layer, correspondingly. The angle θ_3 is related to the angle of incidence θ_0 according to Descartes-Snell's law as follows:

$$n_0\sin\theta_0 = n_1\sin\theta_1, n_1\sin\theta_1 = n_2\sin\theta_2, n_2\sin\theta_2 = n_3\sin\theta_3 \quad (3)$$

Here n_0 is the refractive index of air, n_1, n_2 and n_3 are the real parts of the refractive indices of the PVK, b-Si and c-Si, respectively.

Acceptability of the law of refraction of Descartes-Snell with absorption, i.e. with complex refractive indices of boundary media follows from the following:

According to the "Law of refraction of Descartes-Snell with absorption"[46,47]:

$$\frac{\sin\theta_1}{\sin\theta_2} = \frac{n_2}{n_1}\left(1 - \frac{k_2^2}{n_2^2}\right)$$

For the materials used below (PVK, b-Si, c-Si), the condition $\left(k_2/n_2\right)^2 << 1$ is easily satisfied. It is also necessary to note that in the presence of absorption in the studied media, the properties of the matrix M_j, in particular, the condition $\det M_j$, are preserved under the above-mentioned approximation $\left(k_2/n_2\right)^2 << 1$.

Using the calculation method given in Ref. [29] for reflection and transmission coefficients R and T, we obtain following expressions:

$$R = \frac{(\gamma_0 M_1 - M_3)^2 + (\gamma_0 M_2 - M_4)^2}{(\gamma_0 M_1 + M_3)^2 + (\gamma_0 M_2 + M_4)^2} \quad (4)$$

$$T = \frac{4\gamma_0^2}{(\gamma_0 M_1 + M_3)^2 + (\gamma_0 M_2 + M_4)^2} \quad (5)$$

Absorption coefficient A is then determined as

$$A = 1 - R - T \quad (6)$$

3. Simulation and Analysis

On **Figure 3** shows the reflection, transmission and absorption spectra of the simulated c-Si/b-Si/PVK tandem structure for three different thicknesses of the PVK layer. The analytical expressions of the coefficients M_1, M_2, M_3 and M_4 are given in the Appendix. Numerical calculations were carried out for the wavelength range λ = 0.2-1.2 μm at the angle of incident radiation θ_0 = 60°, assuming the refractive index of air n_0 = 1 and using the following parameters for c-Si, b-Si and PVK: t_1 = 0.4 μm, 0.5 μm and 0.6 μm, t_2 = 0.4 μm, t_3 = 400 μm, n_1 = 2.589[9,48], k_1 = 0.151[9,48], n_2 = 1.2[4], k_2 = 0.067[4,49], n_3 = 3.93[50], k_3 = 0.025[50]. Here, subscripts 1, 2, and 3 denotes the PVK, b-Si, and c-Si layers, respectively (see also **Figure 2**). Because the optical properties of b-Si are similar to those of porous Si, the values of the refractive indices of b-Si (n_2 and k_2) are the same as those of porous Si. The refractive index of b-Si (see porous Si) is lower than that of c-Si[4,49]. As noted in Ref. [51] for PVK-based SCs, the optimal thickness of the perovskite layer is of the order of 0.4-0.8 μm.

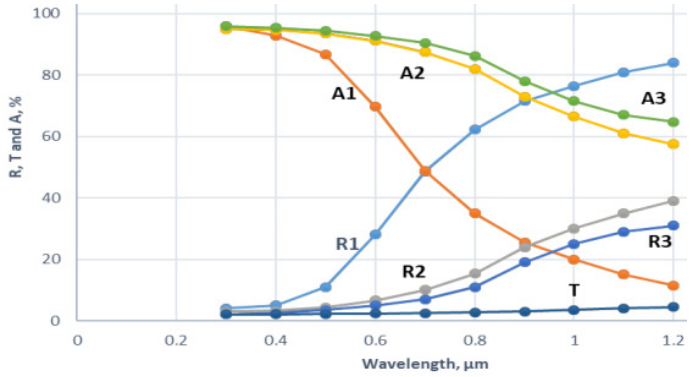

Figure 3. The reflectance, transmittance and absorption spectra of the simulated tandem c-Si/b-Si/PVK structure for three different thicknesses of the PVK layer. By R1, R2 and R3 noted reflectance's, by A1, A2 and A3-acceptance's and by T-transmittance coefficients, correspondingly. The curves R1 and A1 corresponds to case t_1 = 0.4 μm, R2 and A2 corresponds to case t_1 = 0.5 μm, R3 and A3 corresponds to case t_1 = 0.6 μm

The corresponding calculations were carried out using expressions (1)-(6) and using "Microsoft Excel Software". Spectral dependency $A(\lambda)$, $R(\lambda)$ and $T(\lambda)$ determined through the dependencies $L_j = \frac{2\pi}{\lambda}(t_j \cos\theta_j)$ (see Appendix). Note that for the cases t_1 > 0.4 μm, the values of the reflection coefficient in the visible region of the spectrum (up to $\lambda \sim$ 750 nm) were relatively low, less than 10%. This can be explained by the good absorption of all three materials in this spectral range. In the long-wavelength region (at the λ > 0.9 μm), the reflection increases and become 30%-40%. This may be due to both the high reflectivity of c-Si and an increase in reflection at an incidence angle of 60°. The transmittance in all 0.2-1.2 μm range has very low values, less than 5%. At short wavelengths, the absorption has a high value of up to 90%-95% and decreases with increasing wavelength. It is clear that relatively low absorption values in the long-wavelength region are primarily determined by high reflection values, and can also be associated with a decrease in the absorption of the PVK layer (almost 8 times in the wavelength range of 0.45-0.75 μm[51]) and c-Si layer. Note also that reflectance of b-Si, which has very low values in the visible range, increases in the range of 0.4-1.0 μm[3-6]. A slight increase in the thickness of the PVK layer leads to a decrease in the reflectance, which is probably due to an increase in absorption, and this

trend grown with decreasing photon energy.

Figure 4 showed the theoretical curve (for the case t_1 = 0.6 μm) and the measured dependencies of reflectance spectrum of perovskite/TiO_2/b-Si/c-Si tandem samples, taken from Ref. [30]. As we can see, the theoretically modeled curve, both in behavior and magnitude, agrees quite well with the experimental curve PVK/TiO_2/b-Si/Si[30]. The discrepancy between the experimental and model data increases with increasing wavelength. The transmittance was extremely low and increased slowly with the increasing wavelength.

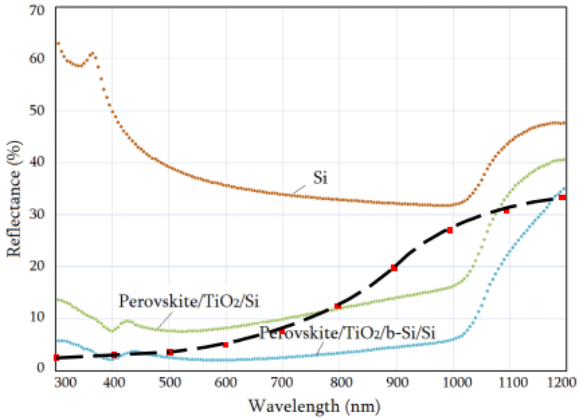

Figure 4. The theoretical curve for the case t_1 = 0.6 μm (black line with red squares) and the measured dependencies of reflectance spectrum of PVK/TiO_2/b-Si/Si tandem samples, taken from Ref. [30]

4. Results and Discussion

The optical properties of a tandem three-layered structure of c-Si/b-Si/PVK have been studied for use in solar energy conversion. The importance and significance of this work is substantiated by the following:

(i) It is shown that the transfer matrix method can be successfully applied to the more complex three-layer case with the complex refractive index of the respective layers.

(ii) The calculation results can be easily extended to other three-layer structures with the selection of new material compositions with modified geometric and optical parameters.

A three-layered structure with the most optimal energy diagram for accumulating solar energy in a wide spectral range is proposed. Numerical calculations performed at an angle of incidence of radiation of 60° showed that in the region of short wavelengths, the reflection coefficient takes on low values, of the order of several percent, and gradually increases and takes on "high" values (> 10%) at wavelengths above 0.8 μm. This can be explained by the deterioration of the absorption by crystalline silicon in the long-wavelength region of the spectrum. The theoretically modeled results of the reflection coefficient are in good agreement with the experimental data carried out for the structures PVK/TiO_2/b-Si/c-Si. Proposed tandem has a high absorption of radiation at short wavelengths in the visible spectrum and can be used to convert solar energy.

Because it is impossible to consider the influence of regular rows of nipples on the b-Si surface on the optical properties within the framework of the transfer matrix method, it is clear that the calculated values for reflection obtained by us will be somewhat larger than the true values. It was assumed that the true reflection values were acceptable for the use of c-Si/b-Si/PVK tandem structure in SCs.

5. Conclusion

The optical properties (reflection, transmission, and absorption) of a tandem three-layer structure are studied using the TMM method, taking into account both real and imaginary parts of the refractive index of all three layers in a wide spectral range. Numerical calculations performed for c-Si/b-Si/PVK have shown that in a wide range of wavelengths the reflection coefficient can take quite low values, on the order of several percent. A good agreement between the calculated data of the reflection coefficient and the experimental data obtained for the PVK/TiO_2/b-Si/c-Si structures is demonstrated. It is proposed to use the PVK/TiO_2/b-Si/c-Si tandem for solar energy conversion.

Acknowledgements

The investigation is carried out with the financial support of the Science Committee of the Republic of Armenia within the framework of Scientific Project No. 21AG-2B011.

Author's Contributions

The whole article is written by me.

Consent for publication

Not applicable.

Availability of Supporting Data

Not applicable.

Conflict of Interest

There is no conflict of interest.

Copyright

References

[1] Khan SB, Irfan S, Zhuanghao Z, *et al.* Influence of refractive index on antireflectance efficiency of thin films. *Materials*, 2019;12(9):1483. https://doi.org/10.3390/ma12091483

[2] Jang SJ, Song YM, Yeo CI, et al. Antireflective property of thin film a-Si solar cell structures with graded refractive index structure. *Optics Express*, 2011;19(102):A108-A117. https://doi.org/10.1364/OE.19.00A108

[3] Ma S, Liu S, Xu Q, *et al*. A theoretical study on the optical properties of black silicon. *AIP Advances*, 2018;8(3):035010. https://doi.org/10.1063/1.5018642

[4] Mei H, Wang C, Yao J, *et al*. Development of novel flexible black silicon. *Optics Communications*, 2011;284(4):1072-1075. https://doi.org/10.1016/j.optcom.2010.10.024

[5] Ayvazyan G, Vaseashta A, Gasparyan F, *et al*. Effect of thermal annealing on the structural and optical properties of black silicon. *Journal of Materials Science: Materials in Electronics*, 2022;33(21):17001-17010. https://doi.org/10.1007/s10854-022-08578-y

[6] Fan Z, Cui D, Zhang Z, *et al*. Recent progress of black silicon: from fabrications to applications. *Nanomaterials*, 2020;11(1):41. https://doi.org/10.3390/nano11010041

[7] Marthi SR, Sekhri S and Ravindra NM. Optical properties of black silicon: an analysis. *Jom*, 2015;67:2154-2159. https://doi.org/10.1007/s11837-015-1527-0

[8] Jurečka S, Králik M, Pinčík E, *et al*. Microstructure and optical properties of black silicon layers. *21st Czech-Polish-Slovak Optical Conference on Wave and Quantum Aspects of Contemporary Optics*, 2018;10976:100-105. https://doi.org/10.1117/12.2518368

[9] Singh JK, Mandal SK and Banerjee G. Refractive index of different perovskite *materials*. *Journal of Materials Research*, 2021;36:1773-1793. https://doi.org/10.1557/s43578-021-00257-8

[10] Lamichhane A and Ravindra NM. Energy gap-refractive index relations in perovskites. *Materials*, 2020;13(8):1917. https://doi.org/10.3390/ma13081917

[11] Ono LK and Qi Y. Research progress on organic–inorganic halide perovskite materials and solar cells. *Journal of Physics D: Applied Physics*, 2018;51(9):093001. https://doi.org/10.1088/1361-6463/aaa727

[12] Ravindra NM, Ganapathy P and Choi J. Energy gap-refractive index relations in semiconductors-an overview. *Infrared Physics & Technology*, 2007;50(1):21-29. https://doi.org/10.1016/j.infrared.2006.04.001

[13] Kumar V, Pandey A, Kumar L, *et al*. Experimental and theoretical investigations on fullerene (C60) induced compact $CH_3NH_3PbI_3$ perovskite thin films. *Physica Scripta*, 2022;97(7):075809. https://doi.org/10.1088/1402-4896/ac74ec

[14] Pandey A and Kumar L. Temperature-induced strain management in $MAPbI_{3-x}Cl_x$ hybrid perovskite films. *Physica B: Condensed Matter*, 2022;628:413566. https://doi.org/10.1016/j.physb.2021.413566

[15] Zhou ZQ, Hu F, Zhou WJ, *et al*. An investigation on a crystalline-silicon solar cell with black silicon layer at the rear. *Nanoscale Research Letters*, 2017;12:1-6. https://doi.org/10.1186/s11671-017-2388-y

[16] Haider M and Yang JL. Efficient and stable perovskite-silicon two-terminal tandem solar cells. *Rare Metals*, 2020;39(7):745-747. https://doi.org/10.1007/s12598-020-01430-4

[17] Kim CU, Yu JC, Jung ED, *et al*. Optimization of device design for low cost and high efficiency planar monolithic perovskite/silicon tandem solar cells. *Nano Energy*, 2019;60:213-221. https://doi.org/10.1016/j.nanoen.2019.03.056

[18] Choi IY, Kim CU, Park W, *et al*. Two-terminal mechanical perovskite/silicon tandem solar cells with transparent conductive adhesives. *Nano Energy*, 2019;65:104044. https://doi.org/10.1016/j.nanoen.2019.104044

[19] Al-Ashouri A, Köhnen E, Li B, *et al*. Monolithic perovskite/silicon tandem solar cell with > 29% efficiency by enhanced hole extraction. *Science*, 2020;370(6522):1300-1309. https://doi.org/10.1126/science.abd4016

[20] Jošt M, Köhnen E, Morales-Vilches AB, *et al*. Textured interfaces in monolithic perovskite/silicon tandem solar cells: advanced light management for improved efficiency and energy yield. *Energy & Environmental Science*, 2018;11(12):3511-3523. https://doi.org/10.1039/C8EE02469C

[21] Wang R, Huang T, Xue J, *et al*. Prospects for metal halide perovskite-based tandem solar cells. *Nature Photonics*, 2021;15(6):411-425. https://doi.org/10.1038/s41566-021-00809-8

[22] Chen B, Zhengshan JY, Manzoor S, *et al*. Blade-coated perovskites on textured silicon for 26%-efficient monolithic perovskite/silicon tandem solar cells. *Joule*, 2020;4(4):850-864. https://doi.org/10.1016/j.joule.2020.01.008

[23] Tennyson EM, Frohna K, Drake WK, *et al*. Multimodal microscale imaging of textured perovskite-silicon tandem solar cells. *ACS Energy Letters*, 2021;6(6):2293-2304. https://doi.org/10.1021/acsenergylett.1c00568

[24] Green MA, Dunlop ED, Yoshita M, *et al*. *Solar cell efficiency tables (version 62)*. National Renewable Energy Laboratory (NREL), Golden, CO (United States), 2023. https://doi.org/10.1002/pip.3726

[25] Ying Z, Yang Z, Zheng J, *et al*. Monolithic perovskite/black-silicon tandems based on tunnel oxide passivated contacts. *Joule*, 2022;6(11):2644-2661. https://doi.org/10.1016/j.joule.2022.09.006

[26] Cheng P, Wang D and Schaaf P. A review on photothermal conversion of solar energy with nanomaterials and nanostructures: From fundamentals to applications. *Advanced Sustainable Systems*, 2022;6(9):2200115. https://doi.org/10.1002/adsu.202200115

[27] Katkov MV, Ayvazyan GY, Shayapov VR, *et al*. Modeling of the optical properties of black silicon passivated by thin films of metal oxides. *Journal of Contemporary Physics (Armenian Academy of Sciences)*, 2020;55:16-22. https://doi.org/10.3103/S106833722001003X

[28] Nishijima Y, Komatsu R, Ota S, *et al*. Anti-reflective surfaces: cascading nano/microstructuring. *Apl Photonics*, 2016;1(7):076104. https://doi.org/10.1063/1.4964851

[29] Gasparyan FV and Ayvazyan GY. Reflection and transmission of radiation of the structure crystalline silicon-black silicon-perovskite. *Journal of Contemporary Physics (Armenian Academy of Sciences)*, 2022;57(2):160-165. https://doi.org/10.3103/S1068337222020116

[30] Ayvazyan G, Gasparyan F and Gasparian V. Optical simulation and experimental investigation of the crystalline silicon/black silicon/perovskite tandem structures. *Optical Materials*, 2023;140:113879. https://doi.org/10.1016/j.optmat.2023.113879

[31] Han K and Chang CH. Numerical modeling of sub-wavelength anti-reflective structures for solar module applications. *Nanomaterials*, 2014;4(1):87-128. https://doi.org/10.3390/nano4010087

[32] Perez EX. Simulation programs for the analysis of multilayer media. *Design, fabrication and characterization of porous silicon multilayer optical devices*. 2007. pp. 27-56.

[33] Kuo ML, Poxson DJ, Kim YS, *et al*. Realization of a near-perfect antireflection coating for silicon solar energy utilization. *Optics Letters*, 2008;33(21):2527-2529. https://doi.org/10.1364/OL.33.002527

[34] Jäger K, Korte L, Rech B, *et al*. Numerical optical optimization of monolithic planar perovskite-silicon tandem solar cells with regular and inverted device architectures. *Optics Express*, 2017;25(12):A473-A482. https://doi.org/10.1364/OE.25.00A473

[35] Raoult E, Bodeux R, Jutteau S, *et al*. Iterative method for optical modelling of perovskite-based tandem solar cells. *Optics Express*, 2022;30(6):9604-9622. https://doi.org/10.1364/OE.444698

[36] van Eerden M, Jaysankar M, Hadipour A, *et al*. Optical analysis of planar multicrystalline perovskite solar cells. *Advanced Optical Materials*, 2017;5(18):1700151. https://doi.org/10.1002/adom.201700151

[37] Sze SM. Physics of semiconductor devices. 2nd ed. Bell Laboratories, Incorporated Murray Hill, New Jersey A Wiley-Interscience. New York. Chichester. Brisbar. Toronto. Singapore. John Wiley & Sons. 1981.

[38] Evtukh AA, Litovchenko VG, Klyui NI, *et al*. Electron field emission from porous silicon prepared at low anodisation currents. *International Journal of Nanotechnology*, 2006;3(1):89-105. https://doi.org/10.1504/IJNT.2006.008723

[39] Martynov YB, Nazmitdinov RG, Moià-Pol A, *et al*. On the efficiency limit of ZnO/$CH_3NH_3PbI_3$/CuI perovskite solar cells. *Physical Chemistry Chemical Physics*, 2017;19(30):19916-19921. https://doi.org/10.1039/C7CP03892E

[40] Chen JZ, Chen TH, Lai LW, *et al*. Preparation and characterization of surface photocatalytic activity with NiO/TiO_2 nanocomposite structure. *Materials*, 2015;8(7):4273-4286. https://doi.org/10.3390/ma8074273

[41] Cui H, Li J and Yuan H. Bending effect on the resistive switching behavior of a NiO/TiO_2 p-n heterojunction. *RSC Advances*, 2018;8(35):19861-19867. https://doi.org/10.1039/C8RA01180J

[42] Uddin MT, Nicolas Y, Olivier C, *et al*. Band alignment investigations of heterostructure NiO/TiO_2 nanomaterials used as efficient heterojunction earth-abundant metal oxide photocatalysts for hydrogen production. *Physical Chemistry Chemical Physics*, 2017;19(29):19279-19288. https://doi.org/10.1039/C7CP01300K

[43] Yeh P, Yariv A and Hong CS. Electromagnetic propagation in periodic stratified media. I. General theory. *Journal of the Optical Society of America*, 1977;67(4):423-438. https://doi.org/10.1364/JOSA.67.000423

[44] Li ZY and Lin LL. Photonic band structures solved by a plane-wave-based transfer-matrix method. *Physical Review E*, 2003;67(4):046607. https://doi.org/10.1103/PhysRevE.67.046607

[45] Hernandez-Rodriguez C, Hernandez VM, Capuj NE, *et al*. Modeling of experimental reflectance for porous silicon multilayers. *Nanotechnology. SPIE*, 2003;5118:577-586. https://doi.org/10.1117/12.498950

[46] Kovalenko SA. Descartes-Snell law of refraction with absorption. *Semiconductor Physics Quantum Electronics & Optoelectronics*, 2001;4(3):214-218. https://doi.org/10.15407/spqeo4.03.214

[47] Kudykina TA. Boundary conditions in case of electromagnetic wave absorption. *Physica Status Solidi (b)*, 1990;160(1):365-373. https://doi.org/10.1002/pssb.2221600136

[48] Löper P, Stuckelberger M, Niesen B, *et al*. Complex refractive index spectra of $CH_3NH_3PbI_3$ perovskite thin films determined by spectroscopic ellipsometry and spectrophotometry. *The Journal of Physical Chemistry Letters*, 2015;6(1):66-71. https://doi.org/10.1021/jz502471h

[49] Singh P, Sharma SN and Ravindra NM. Applications of porous silicon thin films in solar cells and biosensors. *JOM*, 2010;62:15-24. https://doi.org/10.1007/s11837-010-0099-2

[50] Aktsipetrov OA, Baranova IM, Evtyukhov KN. Second order non-linear optics of silicon and silicon nanostructures. 1st ed. Boca Raton: CRC Press; 2016. https://doi.org/10.1201/9781315369556

[51] Du T, Xu W, Xu S, *et al*. Light-intensity and thickness dependent efficiency of planar perovskite solar cells: charge recombination versus extraction. *Journal of Materials Chemistry C*, 2020;8(36):12648-12655. https://doi.org/10.1039/D0TC03390A

Appendix. Supplementary Material

Below are all the parameters that are included in the R, and expressions. They are: M_i, Q_i, q_i, q_i', n_j', k_j', a_j, Γ_j, Γ_j', b_i, c_i and L_i.

$$M_1 = Q_1 + n_3'Q_2' - k_3'Q_2; M_2 = Q_1' - n_3'Q_2 - k_3'Q_2'Q_2;$$

$$M_3 = n_3'Q_4 + k_3'Q_4' + Q_3; M_4 = n_3'Q_4' - k_3'Q_4 - Q_3';$$

$$Q_1 = q_1 - q_2 - q_3 - q_4; Q_1' = q_1' + q_2' + q_3' + q_4';$$

$$Q_2 = q_5 + q_6 + q_7 - q_8; Q_2' = q_5' + q_6' - q_7' + q_8';$$

$$Q_3 = q_9 + q_{10} - q_{11} + q_{12}; Q_3' = q_{10}' + q_{11}' - q_9' - q_{12}';$$

$$Q_4 = q_1 - q_{13} - q_{14} - q_{15}; Q_4' = q_1' + q_{13}' + q_{14}' - q_{15}';$$

$$n_j' = n_j\left(1 - a_j\right), k_j' = k_j\left(1 + a_j\right), a_j = \frac{\left(n_0 \sin\theta_0\right)^2}{n_j^2 + k_j^2};$$

$$\Gamma_j = \frac{n_j'}{\left(n_j'\right)^2 + \left(k_j'\right)^2}; \Gamma_j' = \frac{k_j'}{\left(n_j'\right)^2 + \left(k_j'\right)^2}; \left(j = 1,2,3\right);$$

$$\Gamma_4 = \frac{n_1'n_2' + k_1'k_2'}{\left(n_1'\right)^2 + \left(k_1'\right)^2}; \Gamma_4' = \frac{n_2'k_1' - n_1'k_2'}{\left(n_1'\right)^2 + \left(k_1'\right)^2}; \Gamma_5 = \frac{n_1'n_3' + k_1'k_3'}{\left(n_1'\right)^2 + \left(k_1'\right)^2}; \Gamma_5' = \frac{n_3'k_1' - n_1'k_3'}{\left(n_1'\right)^2 + \left(k_1'\right)^2};$$

$$\Gamma_6 = \frac{n_2'n_3' + k_2'k_3'}{\left(n_2'\right)^2 + \left(k_2'\right)^2}; \Gamma_6' = \frac{n_3'k_2' - n_2'k_3'}{\left(n_2'\right)^2 + \left(k_2'\right)^2}; \Gamma_7 = \frac{n_1'n_2' + k_1'k_2'}{\left(n_2'\right)^2 + \left(k_2'\right)^2}; \Gamma_7' = \frac{n_1'k_2' - n_2'k_1'}{\left(n_2'\right)^2 + \left(k_2'\right)^2};$$

$$\Gamma_8 = \frac{n_1'n_3' + k_1'k_3'}{\left(n_3'\right)^2 + \left(k_3'\right)^2}; \Gamma_8' = \frac{n_1'k_3' - n_3'k_1'}{\left(n_3'\right)^2 + \left(k_3'\right)^2}; \Gamma_9 = \frac{n_2'n_3' + k_2'k_3'}{\left(n_3'\right)^2 + \left(k_3'\right)^2}; \Gamma_9' = \frac{n_2'k_3' - n_3'k_2'}{\left(n_3'\right)^2 + \left(k_3'\right)^2};$$

$$\Gamma_{10} = \frac{n_2'\left(n_1'n_3' - k_1'k_3'\right) + k_2'\left(n_1'k_3' + k_1'n_3'\right)}{\left(n_1'n_3' - k_1'k_3'\right)^2 + \left(n_1'k_3' + k_1'n_3'\right)^2}; \Gamma_{10}' = \frac{n_2'\left(n_1'k_3' + k_1'n_3'\right) - k_2'\left(n_1'n_3' - k_1'k_3'\right)}{\left(n_1'n_3' - k_1'k_3'\right)^2 + \left(n_1'k_3' + k_1'n_3'\right)^2};$$

$$\Gamma_{11} = \frac{n_3'\left(n_1'n_2' + k_1'k_2'\right) + k_3'\left(n_1'k_2' - n_2'k_1'\right)}{\left(n_2'\right)^2 + \left(k_2'\right)^2}; \Gamma_{11}' = \frac{n_3'\left(n_1'k_2' - n_2'k_1'\right) - k_3'\left(n_1'n_2' + k_1'k_2'\right)}{\left(n_2'\right)^2 + \left(k_2'\right)^2};$$

$$b_1 = cos\left(L_1n_1'\right)ch\left(L_1k_1'\right); b_2 = cos\left(L_2n_2'\right)ch\left(L_2k_2'\right);$$

$$b_3 = cos\left(L_3n_3'\right)ch\left(L_3k_3'\right); b_4 = cos\left(L_1n_1'\right)cos\left(L_2n_2'\right);$$

$$b_5 = cos\left(L_3n_3'\right)cos\left(L_2n_2'\right); b_6 = cos\left(L_1n_1'\right)cos\left(L_3n_3'\right);$$

$$b_7 = ch\left(L_1k_1'\right)ch\left(L_2k_2'\right); b_8 = ch\left(L_3k_3'\right)ch\left(L_2k_2'\right);$$

$$b_9 = ch\left(L_1k_1'\right)ch\left(L_3k_3'\right); b_{10} = cos\left(L_1n_1'\right)ch\left(L_2k_2'\right);$$

$$b_{11} = cos\left(L_2n_2'\right)ch\left(L_1k_1'\right); b_{12} = cos\left(n_3'\right)ch\left(L_2k_2'\right);$$

$$b_{13} = cos\left(L_2n_2'\right)ch\left(L_3k_3'\right); b_{14} = cos\left(L_1n_1'\right)ch\left(L_3k_3'\right);$$

$$b_{15} = cos\left(L_3n_3'\right)ch\left(L_1k_1'\right); b_{16} = cos\left(L_3n_3'\right)sh\left(L_3k_3'\right);$$

$$b_{17} = cos\left(L_1n_1'\right)sh\left(L_1k_1'\right); b_{18} = cos\left(L_2n_2'\right)sh\left(L_2k_2'\right);$$

$$c_1 = sin\left(L_1n_1'\right)\mathrm{sh}\left(L_1k_1'\right); c_2 = sin\left(L_2n_2'\right)\mathrm{sh}\left(L_2k_2'\right);$$

$$c_3 = sin\left(L_3n_3'\right)\mathrm{sh}\left(L_3k_3'\right); c_4 = sin\left(L_1n_1'\right)sin\left(L_2n_2'\right);$$

$$c_5 = sin\left(L_3n_3'\right)sin\left(L_2n_2'\right); c_6 = sin\left(L_1n_1'\right)sin\left(L_3n_3'\right);$$

$$c_7 = sh\left(L_1k_1'\right)sh\left(L_2k_2'\right); c_8 = sh\left(L_3k_3'\right)sh\left(L_2k_2'\right);$$

$$c_9 = sh\left(L_1k_1'\right)sh\left(L_3k_3'\right); c_{10} = sin\left(L_1n_1'\right)sh\left(L_2k_2'\right);$$

$$c_{11} = \sin\left(L_2n_2'\right)sh\left(L_1k_1'\right); c_{12} = \sin\left(L_3n_3'\right)\mathrm{sh}\left(L_2k_2'\right);$$

$$c_{13} = sin\left(L_2n_2'\right)sh\left(L_3k_3'\right); c_{14} = sin\left(L_1n_1'\right)sh\left(L_3k_3'\right);$$

$$c_{15} = sin\left(L_3n_3'\right)sh\left(L_1k_1'\right); c_{16} = sin\left(L_3n_3'\right)ch\left(L_3k_3'\right);$$

$$c_{17} = sin\left(L_1n_1'\right)ch\left(L_1k_1'\right); c_{18} = sin\left(L_2n_2'\right)ch\left(L_2k_2'\right);$$

$$q_1 = \text{-}b_3\left(b_1b_2 - c_1c_2\right) + c_3\left(c_1b_2 + c_2b_1\right); q_1' = b_3\left(c_1b_2 + c_2b_1\right) + c_3\left(b_1b_2 - c_1c_2\right);$$

$$q_2 = \Gamma_4\left[c_3\left(b_{10}c_{11} + c_{10}b_{11}\right) + b_3\left(c_4b_7 - b_4c_7\right)\right] - \Gamma_4'\left[c_3\left(c_4b_7 - b_4c_7\right) - b_3\left(b_{10}c_{11} + c_{10}b_{11}\right)\right];$$

$$q_2' = \Gamma_4\left[\mathrm{b}_3\left(b_{10}c_{11} + c_{10}b_{11}\right) - c_3\left(c_4b_7 - b_4c_7\right)\right] - \Gamma_4'\left[c_3\left(b_{10}c_{11} + c_{10}b_{11}\right) + b_3\left(c_4b_7 - b_4c_7\right)\right];$$

$$q_3 = \left(\Gamma_6b_1 - \Gamma_6'c_1\right)\left(c_5b_8 - b_5c_8\right) + \left(\Gamma_6c_1 + \Gamma_6'b_1\right)\left(b_{12}c_{13} + b_{13}c_{12}\right);$$

$$q_3' = \left(\Gamma_6b_1 - \Gamma_6'c_1\right)\left(c_{13}b_{12} + b_{13}c_{12}\right) - \left(\Gamma_6c_1 + \Gamma_6'b_1\right)\left(c_5b_8 - b_5c_8\right);$$

$$q_4 = \left(\Gamma_5 b_2 - \Gamma'_5 c_2\right)\left(c_6 b_9 - b_6 c_9\right) + \left(\Gamma_5 c_2 + \Gamma'_5 b_2\right)\left(b_{14} c_{15} + \mathrm{c}_{14} b_{15}\right);$$

$$q'_4 = \left(\Gamma_5 b_2 - \Gamma'_5 c_2\right)\left(b_{14} c_{15} + c_{14} b_{15}\right) - \left(\Gamma_5 c_2 + \Gamma'_5 b_2\right)\left(c_6 b_9 - b_6 c_9\right);$$

$$q_5 = \left(\Gamma_3 c_{16} + \Gamma'_3 b_{16}\right)\left(b_1 b_2 - c_1 c_2\right) - \left(\Gamma'_3 c_{16} - \Gamma_3 b_{16}\right)\left(c_1 b_2 + c_2 b_1\right);$$

$$q'_5 = \left(\Gamma'_3 c_{16} - \Gamma_3 b_{16}\right)\left(b_1 b_2 - c_1 c_2\right) + \left(\Gamma_3 c_{16} + \Gamma'_3 b_{16}\right)\left(c_1 b_2 + c_2 b_1\right);$$

$$q_6 = \left(\Gamma_2 c_{18} + \Gamma'_2 b_{18}\right)\left(b_1 b_3 - c_1 c_3\right) + \left(\Gamma_2 b_{18} - \Gamma'_2 c_{18}\right)\left(c_1 b_3 + c_3 b_1\right);$$

$$q'_6 = \left(\Gamma_2 c_{18} + \Gamma'_2 b_{18}\right)\left(c_1 b_3 + c_3 b_1\right) - \left(\Gamma_2 b_{18} - \Gamma'_2 c_{18}\right)\left(b_1 b_3 - c_1 c_3\right);$$

$$q_7 = \left(\Gamma_1 c_{17} + \Gamma'_1 b_{17}\right)\left(b_2 b_3 - c_2 c_3\right) + \left(\Gamma_1 b_{17} - \Gamma'_1 c_{17}\right)\left(c_3 b_2 + c_2 b_3\right);$$

$$q'_7 = \left(\Gamma_1 b_{17} - \Gamma'_1 c_{17}\right)\left(b_2 b_3 - c_2 c_3\right) - \left(\Gamma_1 c_{17} + \Gamma'_1 b_{17}\right)\left(c_3 b_2 + c_2 b_3\right);$$

$$q_8 = \Gamma_{10}\left[c_{16}\left(c_4 b_7 - b_4 c_7\right) - b_{16}\left(b_{10} c_{11} + c_{10} b_{11}\right)\right] + \Gamma'_{10}\left[c_{16}\left(b_{10} c_{11} + c_{10} b_{11}\right) + b_{16}\left(c_4 b_7 - b_4 c_7\right)\right];$$

$$q'_8 = \Gamma_{10}\left[b_{16}\left(c_4 b_7 - b_4 c_7\right) + c_{16}\left(b_{10} c_{11} + c_{10} b_{11}\right)\right] + \Gamma'_{10}\left[b_{16}\left(b_{10} c_{11} + c_{10} b_{11}\right) - c_{16}\left(c_4 b_7 - b_4 c_7\right)\right];$$

$$q_9 = \left(n'_1 c_{17} - k'_1 b_{17}\right)\left(b_2 b_3 - c_2 c_3\right) + \left(n'_1 b_{17} + k'_1 c_{17}\right)\left(b_2 c_3 + b_3 c_2\right);$$

$$q'_9 = \left(n'_1 b_{17} + k'_1 c_{17}\right)\left(b_2 b_3 - c_2 c_3\right) - \left(n'_1 c_{17} - k'_1 b_{17}\right)\left(b_2 c_3 + b_3 c_2\right);$$

$$q_{10} = \left(n'_2 c_{18} - k'_2 b_{18}\right)\left(b_1 b_3 - c_1 c_3\right) + \left(n'_2 b_{18} + k'_2 c_{18}\right)\left(c_1 b_3 + c_3 b_1\right);$$

$$q'_{10} = \left(n'_2 c_{18} - k'_2 b_{18}\right)\left(c_1 b_3 + c_3 b_1\right) - \left(n'_2 b_{18} + k'_2 c_{18}\right)\left(b_1 b_3 - c_1 c_3\right);$$

$$q_{11} = \Gamma_{11}\left[c_{16}\left(c_4 b_7 - b_4 c_7\right) - b_{16}\left(b_{10} c_{11} + c_{10} b_{11}\right)\right] + \Gamma'_{11}\left[c_{16}\left(b_{10} c_{11} + c_{10} b_{11}\right) + b_{16}\left(c_4 b_7 - b_4 c_7\right)\right];$$

$$q'_{11} = \Gamma'_{11}\left[c_{16}\left(c_4 b_7 - b_4 c_7\right) - b_{16}\left(b_{10} c_{11} + c_{10} b_{11}\right)\right] + \Gamma_{11}\left[c_{16}\left(b_{10} c_{11} + c_{10} b_{11}\right) + b_{16}\left(c_4 b_7 - b_4 c_7\right)\right];$$

$$q_{12} = \left(n'_3 c_{16} - k'_3 b_{16}\right)\left(b_1 b_2 - c_1 c_2\right) + \left(n'_3 b_{16} + k'_3 c_{16}\right)\left(c_1 b_2 + c_2 b_1\right);$$

$$q'_{12} = \left(n'_3 b_{16} + k'_3 c_{16}\right)\left(b_1 b_2 - c_1 c_2\right) - \left(n'_3 c_{16} - k'_3 b_{16}\right)\left(c_1 b_2 + c_2 b_1\right);$$

$$q_{13} = \left(\Gamma_8 b_3 - \Gamma'_8 c_3\right)\left(c_6 b_9 - b_6 c_9\right) + \left(\Gamma_8 c_3 + \Gamma'_8 b_3\right)\left(b_{14} c_{15} + c_{14} b_{15}\right);$$

$$q'_{13} = \left(\Gamma_8 b_3 - \Gamma'_8 c_3\right)\left(b_{14} c_{15} + c_{14} b_{15}\right) - \left(\Gamma_8 c_3 + \Gamma'_8 b_3\right)\left(c_6 b_9 - b_6 c_9\right);$$

$$q_{14} = \left(\Gamma_9 b_1 - \Gamma'_9 c_1\right)\left(c_5 b_8 - b_5 c_8\right) + \left(\Gamma_9 c_1 + \Gamma'_9 b_1\right)\left(b_{12} c_{13} + c_{12} b_{13}\right);$$

$$q'_{14} = \left(\Gamma_9 b_1 - \Gamma'_9 c_1\right)\left(b_{12} c_{13} + c_{12} b_{13}\right) - \left(\Gamma_9 c_1 + \Gamma'_9 b_1\right)\left(c_5 b_8 - b_5 c_8\right);$$

$$q_{15} = \Gamma_7\left[b_3\left(c_4 b_7 - b_4 c_7\right) + c_3\left(b_{10} c_{11} + c_{10} b_{11}\right)\right] + \Gamma'_7\left[b_3\left(b_{10} c_{11} + c_{10} b_{11}\right) - c_3\left(c_4 b_7 - b_4 c_7\right)\right];$$

$$q'_{15} = \Gamma'_7\left[b_3\left(c_4 b_7 - b_4 c_7\right) + c_3\left(b_{10} c_{11} + c_{10} b_{11}\right)\right] - \Gamma_7\left[b_3\left(b_{10} c_{11} + c_{10} b_{11}\right) - c_3\left(c_4 b_7 - b_4 c_7\right)\right];$$

$$L_1 = 2\pi\lambda\left(t_1 \cos\theta_1\right); L_2 = 2\pi\lambda\left(t_2 \cos\theta_2\right); L_3 = 2\pi\lambda\left(t_3 \cos\theta_3\right)$$